Investigation of aerosol absorption with dual-polarization lidar observations

ZHONGWEI HUANG,[1,2] SIQI QI,[1] TIAN ZHOU,[1,*] QINGQING DONG,[1] XIAOJUN MA,[1] SHUANG ZHANG,[1] JIANRONG BI,[1,2] AND JINSEN SHI[1,2]

[1]*Key Laboratory for Semi-Arid Climate Change of the Ministry of Education, College of Atmospheric Sciences, Lanzhou University, Lanzhou 730000, China*
[2]*Collaborative Innovation Center for West Ecological Safety (CIWES), Lanzhou University, Lanzhou 730000, China*
*zhoutian@lzu.edu.cn

Abstract: Polarization lidar has been widely used in recent decades to observe the vertical structures of aerosols and clouds in the atmosphere. We developed a dual-polarization lidar system that can detect polarization measurements simultaneously at 355 nm and 532 nm. Dust events and haze episodes over northern China in 2014 were observed by the developed lidar. The results showed that the dust-dominated aerosol depolarization ratios at 532 nm were larger than those at 355 nm, but those of the air pollutants were smaller, indicating that this tool could provide a more accurate classification of aerosols. Moreover, we found a good relationship between the absorption coefficient of aerosols and the ratio of depolarization ratios at 532 nm and 355 nm for dust aerosols. Our results imply that aerosol absorption from polarization measurements may be determined by lidar at the ultraviolet and visible wavelengths.

1. Introduction

Atmospheric aerosols can alter the radiative balance of the Earth-atmosphere system by scattering and absorbing shortwave and longwave radiation [1,2]. Aerosol absorption is a significant property driving climate forcing, particularly at the local scale [3]. Black carbon (BC) is known as the main aerosol absorbing light in the atmosphere. Taking light-absorbing BC and non-light absorbing organic carbon as examples, their preferential absorptions at the blue wavelength can be extended to the ultraviolet (UV) wavelength [4]. In addition, there are important contributions from other aerosols, such as unknown brown carbon and mineral dust [5,6].

The absorption of aerosols can be detected by both remote sensing and in situ measurements [5]. For example, Arola et al. [7] presented an approach to correct aerosol absorption results from Ozone Monitoring Instrument (OMI) measurements, combining global aerosol model simulation and Aerosol Robotic Network (AERONET) observations. Satheesh et al. [8] suggested that OMI-Moderate Resolution Imaging Spectroradiometer (MODIS)-Cloud-Aerosol Lidar and Infrared Pathfinder Satellite Observations (CALIPSO) combined observation retrieval has great potential to further improve aerosol absorption detection. Single scattering albedo (SSA), as an important parameter in aerosol absorption, can be retrieved from the ground-based AERONET based on a solar-sky radiometer [9–13]. The measurement of aerosol absorption characteristics could be accurately achieved by various on-site instruments, such as an aethalometer (AE) and multi-angle absorption photometer (MAAP). Real-time mass concentrations of BC can be measured by AE31 [14], a particle soot absorption photometer (PSAP) [15], and MAAP [16]. In addition, the absorption characteristics of BC and dust in snow have been collected and consequently analyzed by using laboratory spectroscopy [17]. However, until now, the vertical profile of aerosol absorption is still very difficult to obtain. Over the past decade, profiles of the

aerosol absorption coefficient were measured by unmanned aerial vehicles (UAVs) [18] and radio sounding balloons [19].

Polarization lidar has been widely used to detect the spatiotemporal distribution of aerosols and clouds in the atmosphere [20–27]. Sugimoto et al. [28] found a mixture of dust and sulfate in the upper boundary layer during dust events and anthropogenic aerosol plumes in the Northwest Pacific. Groß et al. [29] reported vertical distribution of the Saharan dust after long-range transport across the Atlantic Ocean by use of a dual-wavelength polarization lidar. Janicka et al. [30] analyzed polarization measurements of simultaneous advection of Saharan dust and the Canadian biomass burning aerosol in well separated in time and space layers over Warsaw in July 2013. It is well known that particle types can be identified from polarization measurements [22,31–34]. Liu et al. [35] investigated the characterization of dust in the troposphere by using layer-averaged depolarization ratios (DRs) from CALIPSO lidar observations. Zhou et al. [36] identified dust plumes over the Taklimakan Desert using the relationship between the layer-integrated attenuated backscatter coefficient and layer-integrated DR. Burton et al. [37] proposed a parameterization scheme that can divide aerosols into two or more types by using polarization lidar measurements. In addition, spectral DRs of particles have also been reported in the literature. For dust-dominated aerosols, the DRs at 532 nm are larger than those at 355 nm but are smaller for smoke particles [38]. The reason for this phenomenon is likely related to the absorption of particles [39,40].

In this study, we developed a dual-polarization lidar system aimed at investigating the relationship between the DRs of atmospheric aerosols at UV and visible (VIS) wavelengths. Moreover, the identification of aerosol types is achieved based on spectral polarization measurements. We attempted to determine the relationship between the DRs and the absorption of dust aerosols. Section 2 briefly introduces the developed lidar system and methods used in this paper. The results and discussions are described in Section 3. Finally, the conclusion is given in Section 4.

2. Instruments and observational data

2.1. Dual-polarization lidar system

We developed a ground-based dual-polarization lidar system for observing the vertical structure of aerosols and clouds in the troposphere. The developed lidar employs a flash-lamp-pumped, third /second-harmonic Nd:YAG laser with two wavelengths of 532 nm and 355 nm. Then, the backscattering signal from the atmosphere was collected by a receiver telescope with a diameter of 350 mm. The polarization measurements were detected at 532 nm and 355 nm simultaneously. Licel transient recorders were used to simultaneously measure multichannel signals in analog mode and photons counting. The DR at each wavelength was calculated by the ratio of the parallel and perpendicular components of the backscattering signals, consequently incomplete overlap can be eliminated. It is noted that overlap problem could be solved by use of Scheimpflug lidar system [41]. To compare lidar measurements with co-located ground-based absorption observation, the overlap height of the developed lidar was set to very low (~50 meters). The spatial resolution and temporal resolution of the lidar system were 3.75 meters and 2 min, respectively. The lidar measurements of dust aerosols and air pollutants in the atmosphere over northern China in 2014 were used in this study.

2.2. Multiangle absorption photometer (MAAP)

The MAAP (model-5012, Thermo Scientific, USA) is a single wavelength (637 nm) instrument with a half maximum width of 18 nm [42]. The transmittance of the filter and scattering from two angles (130° and 165°) are monitored by using a two-stream radiation transfer model with a glass fiber filter band (GF-10, Thermo Fisher Science, USA) [16,43]. Without the influence of scattering particles, the absorbance of deposited particles is determined. The absorption

coefficient measured by the MAAP is expressed in terms of BC mass concentration. The reference absorption coefficient is calculated by measuring the difference between the extinction coefficient and scattering coefficient and by photoacoustic photometry. The advantages of these methods are that the particles can be sampled for a long time to improve the filter, which not only collects particles on the actual surface of the filter but also penetrates far below the limit of the detectable absorption coefficient of 1 Mm^{-1}. Using this filter, even for particles less than 100 nm, the deposition efficiency is very high, and the process of sampling is simple [43]. The MAAP is currently a relatively simple means of automatically and continuously observing BC. To ensure the accuracy of the data before measurement, the instrument should be calibrated for temperature, pressure and flow. In this paper, the aerosol absorption coefficient σ_{ab} (Mm^{-1}) is obtained by using the empirical conversion factor of BC (6.6 m^2/g), as reported by Hitzenberger et al. [44]:

$$\sigma_{ab} = 6.6 M_{BC}. \tag{1}$$

where M_{BC} is the concentration of BC.

3. Results and discussion

Dust storms usually occur over east Asia in late winter and springtime and have significant impacts on the regional climate, environment and ecosystem [45,46]. On April 12-13, 2014, a heavy dust storm originating from the Taklimakan Desert occurred over northern China and was observed by the developed dual-polarization lidar system. The vertical structure of atmospheric aerosols and clouds from lidar observations in Linze (39.14°N, 100.17°E) during the dust event on April 13, 2014, is shown in the left panel of Fig. 1. The lidar observations of another dust case in Zhongmou (34.73°N, 114.00°E) on December 14, 2014, are shown in the right panel of Fig. 1. The attenuated backscattering coefficients (ABC) and DRs at 532 and 355 nm are shown. There was a dust event on the afternoon of April 13 in Linze according to the high ABC and DR values at 532 nm from the lidar measurements. However, the results show a small DR value at 355 nm during the dust event. Moreover, it is noted that for dust particles the ABCs at 532 nm are larger than those at 355 nm, also as reported by previous studies [e.g., 47–49]. The reason may be due to absorption of dust particles [47]. This finding was confirmed from lidar measurements observed by another lidar system for a dust case in Zhongmou on December 14, 2014. We can see that multilayer dust aerosols were found between 1 km and 3 km at a height above ground level. The same phenomenon, where the DR value at 532 nm was larger than that at 355 for dust-dominated particles, still clearly existed. Air pollutants were also observed below 1 km during this dust event. However, we can see that for air pollutants, the DR value at 532 nm was smaller than that at 355 nm. These phenomena regarding the spectral DRs of dust aerosols and air pollutants are quite different, which has also been reported by previous studies [38,40].

The identification of aerosol types has been studied over past decades based on lidar measurements [37,50,51]. Aerosol classification can be markedly improved by using high-spectral-resolution lidar (HSRL), especially by employing polarization measurements at different wavelengths [31,37,38]. In this study, we used the ratio of the DRs at 532 nm and 355 nm to classify the aerosol types more effectively. The relationship between the DRs at 532 nm and 355 nm and the DR at 532 nm is shown for two typical aerosol types (dust and air pollutants) in Fig. 2. The data points were selected from red boxes as marked in Fig. 1. We can see that these two aerosol types can be obviously separated using this relation. For dust aerosols, the DR at 532 nm is larger than 0.22, and the ratio of the DRs at 532 nm and 355 nm is greater than 1.1. However, for anthropogenic air pollutants, the DR at 532 nm is smaller than 0.16, and the ratio of the DRs at 532 nm and 355 nm is less than 0.8. According to this pattern, the ratio of the DRs at 532 nm and 355 nm ranges from 0.8 to 1.1, while the DR at 532 nm is attributed to a mixture of dust and air pollutants. The average values of DR for dust aerosols are 0.25 ± 0.03 (532 nm) and 0.20 ± 0.02 (355 nm) respectively, but for anthropogenic air pollutants are 0.14 ± 0.01 (532
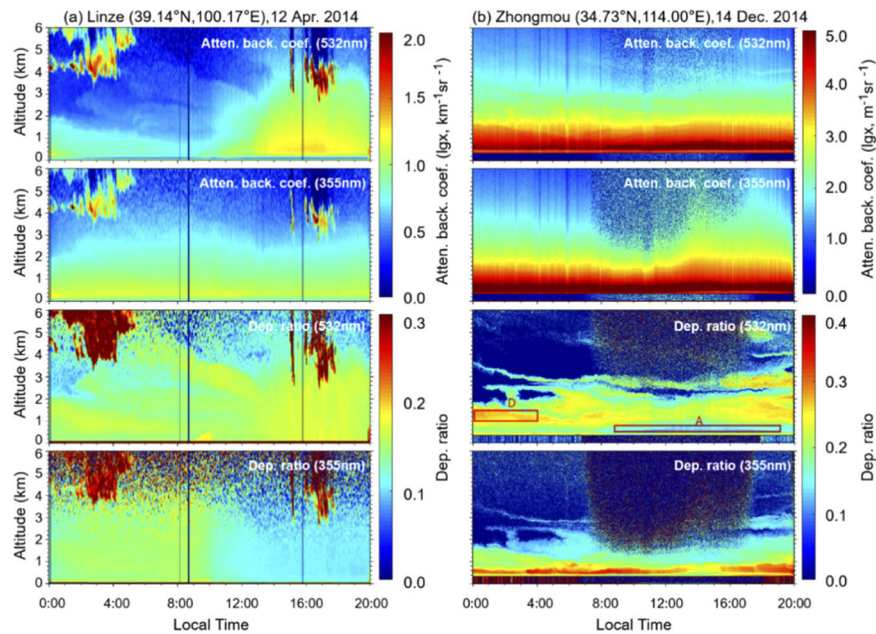
Fig. 1. Vertical structure of atmospheric aerosols and clouds from lidar observation. Left panel: dust case in Linze (39.14°N, 100.17°E) on April 13, 2014. Right panel: case of dust and air pollutant mixing in Zhongmou (34.73°N, 114.00°E) on December 14, 2014. The data points of dust aerosols (D) and air pollutants (A) in Fig. 2 are marked by red boxes.

nm) and 0.27 ± 0.02 (355 nm). Following this idea, we identified aerosol types based on lidar measurements in Zhongmou on December 14, 2014, as shown in Fig. 3. The results show that there was multilayer aerosol mixing during the observation time. Moreover, dust aerosols can be clearly seen as mixing with air pollutants within the boundary layer. Therefore, dual-polarization measurements can be used to largely improve aerosol classification.
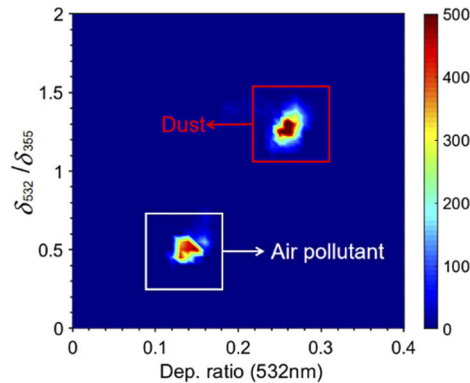

Fig. 2. Probability distribution function (PDF) of dust aerosols and air pollutants for the relationship between the DR (532 nm) and ratio of DRs at 532 nm and 355 nm from lidar measurements of Zhongmou on December 14, 2014. The grid resolution is 40×40.

To investigate the reason why different DRs are observed at 532 nm and 355 nm for aerosols, we studied the relationship between the ratio of the DRs at the two wavelengths from the lidar measurements and the aerosol absorption coefficient from the independent observations. To
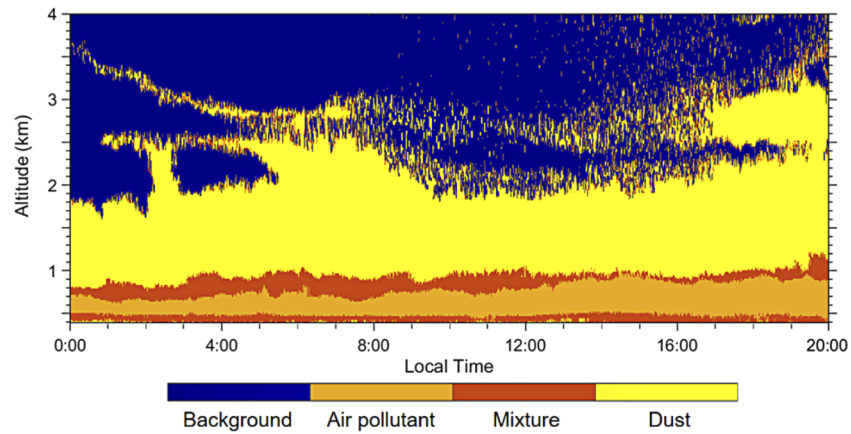
Fig. 3. Vertical distribution of aerosol identification using dual-polarization lidar measurements in Zhongmou on December 14, 2014. The temporal and spatial resolutions are 1 min and 19 m, respectively.

compare with the surface aerosol absorption coefficient observed by the colocated MAAP, lidar measurements between 70 and 100 meters were used and averaged. Figure 4 shows that the aerosol absorption coefficient observed by the MAAP in Zhangye on April 12, 2014, decreased with increasing DR ratio at the two wavelengths for dust aerosols. The correlation coefficient R is 0.71, and the standard root mean square error (RMSE) is 2.11. The difference in DR between 532 and 355 nm may be caused by the absorption characteristics of aerosols [38,39]. Previous studies have proven that dust aerosols show substantial absorption characteristics. The amount of dust absorption varies with particle size distribution, composition and shape [52,53]. In addition, the absorption of dust aerosols has been studied from AERONET sun-photometer observations over northwestern China [54–56]. It is worth noting that dust particles accounted for approximately 26.7% of aerosol absorption during floating dust events but increased to 71.6% during heavy dust storms over northwestern China [57]. Therefore, it can be concluded that the absorption characteristics of dust aerosols cause a difference in the DR at the UV and VIS wavelengths.
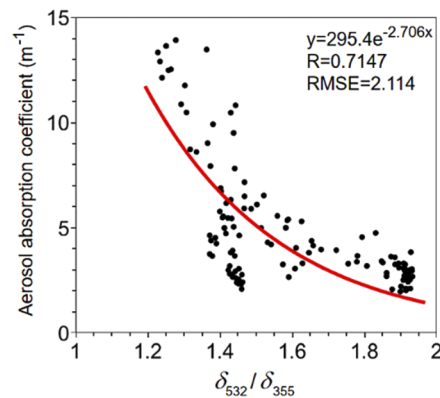

Fig. 4. The relationship between the aerosol absorption coefficient observed by a colocated MAAP and the ratio of the DRs at 532 nm and 355 nm from lidar measurements in Zhangye on April 12, 2014, during the dust event.

4. Conclusion

To obtain more information from polarization lidar measurements, we developed a dual-polarization lidar system that can detect polarization measurements simultaneously at both 355 nm and 532 nm. The vertical distributions of atmospheric aerosols and clouds over northern China were successfully observed by the developed lidar. Observational data during two typical cases (dust events and haze episodes) were used for the analysis in this study. The results showed that for dust-dominated aerosols, the DR at 532 nm was larger than that at 355 nm, but that for air pollutants was smaller. This can provide more information for the accurate classification of aerosol types. Our results show that dual-polarization measurements can be used to largely improve aerosol classification. Moreover, we found that there is a good relationship between the absorption coefficient of aerosols and the ratio of DRs at 532 nm and 355 nm for dust aerosols. These results confirm that the absorption characteristics of dust aerosols cause a difference in DR at the UV and VIS wavelengths. In the future, aerosol absorption may be obtained from lidar spectral polarization measurements.

Disclosures

The authors declare that there are no conflicts of interest related to this article.

References

1. O. Boucher and J. Haywood, "Estimates of the Direct and Indirect Radiative Forcing Due to Tropospheric Aerosols: A Review," Rev. Geophys. **38**(4), 513–543 (2000).
2. Z. Huang, J. Huang, J. Bi, G. Wang, W. Wang, Q. Fu, Z. Li, S.-C. Tsay, and J. Shi, "Dust aerosol vertical structure measurements using three MPL lidars during 2008 China-U.S. joint dust field experiment," J. Geophys. Res. **115**(D7), D00K15 (2010).
3. B. A. Bodhaine, "Aerosol absorption measurements at Barrow, Mauna Loa and aerosol have also been measured continuously for many years is consistent with specific absorption of BC on the aethalometer specific absorption atmosphere measurements of the wavelength dependence," J. Geophys. Res. **100**(D5), 8967–8975 (1995).
4. C. Bond, "Spectral dependence of visible light absorption by carbonaceous particles emitted from coal combustion," Geophys. Res. Lett. **28**(21), 4075–4078 (2001).
5. H. Moosmüller, R. K. Chakrabarty, and W. P. Arnott, "Aerosol light absorption and its measurement: A review," J. Quant. Spectrosc. Radiat. Transfer **110**(11), 844–878 (2009).
6. A. Petzold, K. Rasp, B. Weinzierl, M. Esselborn, T. Hamburger, A. Dörnbrack, K. Kandler, L. Schütz, P. Knippertz, M. Fiebig, and A. Virkkula, "Saharan dust absorption and refractive index from aircraft-based observations during SAMUM 2006," Tellus B **61**(1), 118–130 (2009).
7. A. Arola, S. Kazadzis, A. Lindfors, N. Krotkov, J. Kujanpää, J. Tamminen, A. Bais, A. di Sarra, J. M. Villaplana, C. Brogniez, A. M. Siani, P. Weihs, A. Webb, T. Koskela, N. Kouremeti, D. Meloni, V. Buchard, F. Auriol, I. Ialongo, M. Staneck, S. Simic, A. Smedley, and S. Kinne, "A new approach to correct for absorbing aerosols in OMI UV," Geophys. Res. Lett. **36**(22), L22805 (2009).
8. S. K. Satheesh, O. Torres, L. A. Remer, S. S. Babu, V. Vinoj, T. F. Eck, R. G. Kleidman, and B. N. Holben, "Improved assessment of aerosol absorption using OMI-MODIS joint retrieval," J. Geophys. Res. **114**(D5), 1–10 (2009).
9. D. M. Giles, B. N. Holben, T. F. Eck, A. Sinyuk, A. Smirnov, I. Slutsker, R. R. Dickerson, A. M. Thompson, and J. S. Schafer, "An analysis of AERONET aerosol absorption properties and classifications representative of aerosol source regions," J. Geophys. Res.: Atmos. **117**(17), D17203 (2012).
10. J. Li, B. E. Carlson, and A. A. Lacis, "Using single-scattering albedo spectral curvature to characterize East Asian aerosol mixtures," J. Geophys. Res.: Atmos. **120**(5), 2037–2052 (2015).

11. R. P. Pokhrel, N. L. Wagner, J. M. Langridge, D. A. Lack, T. Jayarathne, E. A. Stone, C. E. Stockwell, R. J. Yokelson, and S. M. Murphy, "Parameterization of single-scattering albedo (SSA) and absorption Ångström exponent (AAE) with EC/OC for aerosol emissions from biomass burning," Atmos. Chem. Phys. **16**(15), 9549–9561 (2016).

12. P. B. Russell, R. W. Bergstrom, Y. Shinozuka, A. D. Clarke, P. F. Decarlo, J. L. Jimenez, J. M. Livingston, J. Redemann, O. Dubovik, and A. Strawa, "Absorption Angstrom Exponent in AERONET and related data as an indicator of aerosol composition," Atmos. Chem. Phys. **10**(3), 1155–1169 (2010).

13. J. Bi, J. Huang, Z. Hu, B. N. Holben, and Z. Guo, "Investigating the aerosol optical and radiative characteristics of heavy haze episodes in Beijing during January of 2013," J. Geophys. Res.: Atmos. **119**(16), 9884–9900 (2014).

14. T. A. Rajesh and S. Ramachandran, "Black carbon aerosol mass concentration, absorption and single scattering albedo from single and dual spot aethalometers: Radiative implications," J. Aerosol Sci. **119**, 77–90 (2018).

15. J. Backman, A. Virkkula, V. Vakkari, J. P. Beukes, P. G. Van Zyl, M. Josipovic, S. Piketh, P. Tiitta, K. Chiloane, T. Petäjä, M. Kulmala, and L. Laakso, "Differences in aerosol absorption Ångström exponents between correction algorithms for a particle soot absorption photometer measured on the South African Highveld," Atmos. Meas. Tech. **7**(12), 4285–4298 (2014).

16. Y. Kanaya, F. Taketani, Y. Komazaki, X. Liu, Y. Kondo, L. K. Sahu, H. Irie, and H. Takashima, "Comparison of black carbon mass concentrations observed by multi-angle absorption photometer (MAAP) and continuous soot-monitoring system (COSMOS) on fukue Island and in Tokyo, Japan," Aerosol Sci. Technol. **47**(1), 1–10 (2013).

17. X. Wang, S. J. Doherty, and J. Huang, "Black carbon and other light-absorbing impurities in snow across Northern China," J. Geophys. Res.: Atmos. **118**(3), 1471–1492 (2013).

18. M. V. Ramana, V. Ramanathan, D. Kim, G. C. Roberts, and C. E. Corrigan, "Albedo, atmospheric solar absorption and heating rate measurements with stacked UAVs," Q. J. R. Meteorol. Soc. **133**(629), 1913–1931 (2007).

19. A. Maletto, I. G. McKendry, and K. B. Strawbridge, "Profiles of particulate matter size distributions using a balloon-borne lightweight aerosol spectrometer in the planetary boundary layer," Atmos. Environ. **37**(5), 661–670 (2003).

20. F. Cairo, G. Di Donfrancesco, A. Adriani, L. Pulvirenti, and F. Fierli, "Comparison of various linear depolarization parameters measured by lidar," Appl. Opt. **38**(21), 4425–4432 (1999).

21. G. J. Kunz, "Two-wavelength lidar inversion algorithm," Appl. Opt. **38**(6), 1015–1020 (1999).

22. J. Lee, J. Kim, C. H. Song, J. H. Ryu, Y. H. Ahn, and C. K. Song, "Algorithm for retrieval of aerosol optical properties over the ocean from the Geostationary Ocean Color Imager," Remote Sens. Environ. **114**(5), 1077–1088 (2010).

23. T. Murayama, D. Müller, K. Wada, A. Shimizu, M. Sekiguchi, and T. Tsukamoto, "Characterization of Asian dust and Siberian smoke with multi-wavelength Raman lidar over Tokyo, Japan in spring 2003," Geophys. Res. Lett. **31**(23), 1–5 (2004).

24. N. Sugimoto, Z. Huang, T. Nishizawa, I. Matsui, and B. Tatarov, "Fluorescence from atmospheric aerosols observed with a multi-channel lidar spectrometer," Opt. Express **20**(19), 20800–20807 (2012).

25. N. Sugimoto and Z. Huang, "Lidar methods for observing mineral dust," J. Meteorol. Res. **28**(2), 173–184 (2014).

26. J. P. Huang, J. J. Liu, B. Chen, and S. L. Nasiri, "Detection of anthropogenic dust using CALIPSO lidar," Atmos. Chem. Phys. **15**(20), 11653–11665 (2015).

27. W. Wang, J. Huang, P. Minnis, Y. Hu, J. Li, Z. Huang, J. K. Ayers, and T. Wang, "Dusty cloud properties and radiative forcing over dust source and downwind regions derived from A - Train data during the Pacific Dust Experiment," J. Geophys. Res. **115**(D4), 1–17 (2010).

28. N. Sugimoto, I. Matsui, A. Shimizu, I. Uno, K. Asai, T. Endoh, and T. Nakajima, "Observation of dust and anthropogenic aerosol plumes in the Northwest Pacific with a two-wavelength polarization lidar on board the research vessel Mirai," Geophys. Res. Lett. **29**(19), 7-1–7-4 (2002).

29. S. Groß, V. Freudenthaler, K. Schepanski, C. Toledano, A. Schäfler, A. Ansmann, and B. Weinzierl, "Optical properties of long-range transported Saharan dust over Barbados as measured by dual-wavelength depolarization Raman lidar measurements," Atmos. Chem. Phys. **15**(19), 11067–11080 (2015).

30. L. Janicka, I. S. Stachlewska, I. Veselovskii, and H. Baars, "Temporal variations in optical and microphysical properties of mineral dust and biomass burning aerosol derived from daytime Raman lidar observations over Warsaw, Poland," Atmos. Environ. **169**, 162–174 (2017).

31. S. P. Burton, R. A. Ferrare, C. A. Hostetler, J. W. Hair, R. R. Rogers, M. D. Obland, C. F. Butler, A. L. Cook, D. B. Harper, and K. D. Froyd, "Aerosol classification using airborne High Spectral Resolution Lidar measurements-methodology and examples," Atmos. Meas. Tech. **5**(1), 73–98 (2012).

32. A. J. Illingworth, H. W. Barker, A. Beljaars, M. Ceccaldi, H. Chepfer, N. Clerbaux, J. Cole, J. Delanoë, C. Domenech, D. P. Donovan, S. Fukuda, M. Hirakata, R. J. Hogan, A. Huenerbein, P. Kollias, T. Kubota, T. Nakajima, T. Y. Nakajima, T. Nishizawa, Y. Ohno, H. Okamoto, R. Oki, K. Sato, M. Satoh, M. W. Shephard, A. Velázquez-Blázquez, U. Wandinger, T. Wehr, and G.-J. van Zadelhoff, "The EarthCARE Satellite: The Next Step Forward in Global Measurements of Clouds, Aerosols, Precipitation, and Radiation," Bull. Am. Meteorol. Soc. **96**(8), 1311–1332 (2015).

33. Y. Noh, D. Müller, K. Lee, K. Kim, K. Lee, A. Shimizu, I. Sano, and C. B. Park, "Depolarization ratios retrieved by AERONET sun–sky radiometer data and comparison to depolarization ratios measured with lidar," Atmos. Chem. Phys. **17**(10), 6271–6290 (2017).

34. S. Groß, M. Esselborn, B. Weinzierl, M. Wirth, A. Fix, and A. Petzold, "Aerosol classification by airborne high spectral resolution lidar observations," Atmos. Chem. Phys. **13**(5), 2487–2505 (2013).

35. Z. Liu, A. Omar, M. Vaughan, J. Hair, C. Kittaka, Y. Hu, K. Powell, C. Trepte, D. Winker, C. Hostetler, R. Ferrare, and R. Pierce, "CALIPSO lidar observations of the optical properties of Saharan dust: A case study of long-range transport," J. Geophys. Res.: Atmos. **113**(7), 1–20 (2008).

36. T. Zhou, J. Huang, Z. Huang, J. Liu, W. Wang, and L. Lin, "The depolarization–attenuated backscatter relationship for dust plumes," Opt. Express **21**(13), 15195 (2013).

37. S. P. Burton, M. A. Vaughan, R. A. Ferrare, and C. A. Hostetler, "Separating mixtures of aerosol types in airborne High Spectral Resolution Lidar data," Atmos. Meas. Tech. **7**(2), 419–436 (2014).

38. S. P. Burton, J. W. Hair, M. Kahnert, R. A. Ferrare, C. A. Hostetler, A. L. Cook, D. B. Harper, T. A. Berkoff, S. T. Seaman, J. E. Collins, M. A. Fenn, and R. R. Rogers, "Observations of the spectral dependence of linear particle depolarization ratio of aerosols using NASA Langley airborne High Spectral Resolution Lidar," Atmos. Chem. Phys. **15**(23), 13453–13473 (2015).

39. S. Groß, V. Freudenthaler, M. Wirth, and B. Weinzierl, "Towards an aerosol classification scheme for future EarthCARE lidar observations and implications for research needs," Atmos. Sci. Lett. **16**(1), 77–82 (2015).

40. M. I. Mishchenko, J. M. Dlugach, and L. Liu, "Linear depolarization of lidar returns by aged smoke particles," Appl. Opt. **55**(35), 9968–9973 (2016).

41. L. Mei and M. Brydegaard, "Atmospheric aerosol monitoring by an elastic Scheimpflug lidar system," Opt. Express **23**(24), A1613–A1628 (2015).

42. T. Müller, J. S. Henzing, G. De Leeuw, A. Wiedensohler, A. Alastuey, H. Angelov, and M. Bizjak, "Characterization and intercomparison of aerosol absorption photometers: result of two intercomparison workshops," Atmos. Meas. Tech. **4**(2), 245–268 (2011).

43. A. Petzold and M. Schönlinner, "Multi-angle absorption photometry - A new method for the measurement of aerosol light absorption and atmospheric black carbon," J. Aerosol Sci. **35**(4), 421–441 (2004).

44. R. Hitzenberger, A. Petzold, H. Bauer, P. Ctyroky, P. Pouresmaeil, L. Laskus, and H. Puxbaum, "Intercomparison of thermal and optical measurement methods for elemental carbon and black carbon at an urban location," Environ. Sci. Technol. **40**(20), 6377–6383 (2006).

45. Z. Huang, J. B. Nee, C. W. Chiang, S. Zhang, H. Jin, W. Wang, and T. Zhou, "Real-time observations of dust-cloud interactions based on polarization and Raman lidar measurements," Remote Sens. **10**(7), 1–14 (2018).

46. Z. Huang, J. Huang, T. Hayasaka, S. Wang, and T. Zhou, "Short-cut transport path for Asian dust directly to the Arctic: A case study Short-cut transport path for Asian dust directly to the Arctic: a case study," Environ. Res. Lett. **10**(11), 114018 (2015).

47. I. Mattis, A. Ansmann, D. Müller, U. Wandinger, and D. Althausen, "Dual-wavelength Raman lidar observations of the extinction-to-backscatter ratio of Saharan dust," Geophys. Res. Lett. **29**(9), 20-1–20-4 (2002).

48. J. Hofer, D. Althausen, S. F. Abdullaev, A. N. Makhmudov, B. I. Nazarov, G. Schettler, R. Engelmann, H. Baars, K. W. Fomba, K. Müller, B. Heinold, K. Kandler, and A. Ansmann, "Long-term profiling of mineral dust and pollution aerosol with multiwavelength polarization Raman lidar at the Central Asian site of Dushanbe, Tajikistan: case studies," Atmos. Chem. Phys. **17**(23), 14559–14577 (2017).

49. B. Liu, Y. Ma, W. Gong, and M. Zhang, "Observations of aerosol color ratio and depolarization ratio over wuhan," Atmos. Pollut. Res. **8**(6), 1113–1122 (2017).

50. M. Haarig, A. Ansmann, H. Baars, C. Jimenez, I. Veselovskii, R. Engelmann, and D. Althausen, "Depolarization and lidar ratios at 355, 532, and 1064 nm and microphysical properties of aged tropospheric and stratospheric Canadian wildfire smoke," Atmos. Chem. Phys. **18**(16), 11847–11861 (2018).

51. S. Shin, Y. M. Noh, K. Lee, H. Lee, D. Müller, Y. J. Kim, K. Kim, and D. Shin, "Retrieval of the single scattering albedo of Asian dust mixed with pollutants using lidar observations," Adv. Atmos. Sci. **31**(6), 1417–1426 (2014).

52. I. N. Sokolik and O. B. Toon, "Incorporation of mineralogical composition into models of the radiative properties of mineral aerosol from UV to IR wavelengths," J. Geophys. Res. Atmos. **104**(D8), 9423–9444 (1999).

53. I. Mattis, A. Ansmann, D. Müller, U. Wandinger, and D. Althausen, "Dual-wavelength Raman lidar observations of the extinction-to-backscatter ratio of Saharan dust," Geophys. Res. Lett. **29**(9), 20-1–20-4 (2002).

54. T. Zhou, H. Xie, J. Bi, Z. Huang, J. Huang, J. Shi, B. Zhang, and W. Zhang, "Lidar Measurements of Dust Aerosols during Three Field Campaigns in 2010, 2011 and 2012 over Northwestern China," Atmosphere **9**(5), 173 (2018).

55. J. Bi, J. Huang, B. Holben, and G. Zhang, "Comparison of key absorption and optical properties between pure and transported anthropogenic dust over East and Central Asia," Atmos. Chem. Phys. **16**(24), 15501–15516 (2016).

56. J. Bi, J. Huang, J. Shi, Z. Hu, T. Zhou, G. Zhang, Z. Huang, X. Wang, and H. Jin, "Measurement of scattering and absorption properties of dust aerosol in a Gobi farmland region of northwestern China – a potential anthropogenic influence," Atmos. Chem. Phys. **17**(12), 7775–7792 (2017).

57. X. Wu, J. Liu, Y. Wu, X. Wang, X. Yu, J. Shi, J. Bi, Z. Huang, T. Zhou, and R. Zhang, "Aerosol optical absorption coefficients at a rural site in Northwest China: The great contribution of dust particles," Atmos. Environ. **189**, 145–152 (2018).